OPEN ACCESS Freely available online

ISSN 2737-5323
Volume 1, Issue 1
https://www.iikii.com.sg/journal/AFM
Applied Functional Materials

Article

Silica as a Scaffold Layer via Electrospray for $MAPbI_3$ Perovskite-based Solar Cell

Chun-Chih Hu, Ting-Yu Tai, Chi-Wei Chan and Yaw-Shyan Fu*

Department of Greenergy, National University of Tainan, Tainan 700, Taiwan.
* Correspondence: ysfu@mail.nutn.edu.tw

Received: May 15, 2021; **Accepted:** Jun 17, 2021; **Published:** Jul 31, 2021

Abstract: We synthesized a novel hybridized perovskite-silica (SiO_2) solar cell using an electrospray process under ambient conditions. The Silica scaffold not only provided optical transmission from visible to infrared regions but also blocked the back flow transport of the holes and electrons to reach the electrodes, leading to reduced charge recombination. Moreover, the $CH_3NH_3PbI_3$ ($MAPbI_3$) film quality can be improved by using the combination of vacuum annealing enhanced crystal growth and the methylamine (CH_3NH_2, MA) vapor-assisted diffusion at the grain boundaries, due to reduced surface roughness and the re-crystallization of the $MAPbI_3$ film. Photovoltaic performances were evaluated using the glass/ITO/poly (3,4-ethylenedioxythiophene) poly(styrene-sulfonate) (PEDOT:PSS)/SiO_2/$MAPbI_3$/C_{60}/BCP/Al device structure, with the champion $MAPbI_3$ based perovskite-silica solar cell exhibited a short-circuit current density of 19.89 mA/cm^2, an open-circuit voltage of 0.89 V, a fill factor of 0.50, and a power conversion efficiency of 8.85%.

Keywords: Perovskite; SiO_2; Electrospray; Crystal growth; $MAPbI_3$

1. Introduction

To date, organic-inorganic perovskite materials with chemical formula ABX_3 (where A is organic cation, alkali; B is Ge, Sn, or Pb and X is halide) have been investigated for solar cells applications. These lead halide perovskite materials are highly promising solar cell absorber material due to their direct energy gap, high optical absorption coefficient of 10^4~10^5 cm^{-1}, high carrier mobility of 10 cm^2 V^{-1}s^{-1}, long electron-hole diffusion lengths [1-3], low temperatures processing, and outstanding photoelectric properties [4–6]. Recent reports have shown that both single and multiple solution processes [7-9] and vapor-induced reaction method [10-11] yield solar cells with high power conversion efficiency for various device structures. Generally, perovskite-based solar cells are fabricated with n-i-p mesoscopic TiO_2 [12-14], super-meso structures Al_2O_3 or SnO_2 scaffold [15-16] and a compact hole-blocking layer TiO_2/ZnO/TiO_2 multi-layer [17]. Yi, et al. was demonstrated that the $LaCoO_3$ perovskite makes possible the convenient and rapid generation of SBA-15-hosted perovskite nanocrystals with favorable microstructural modification, resulting in the creation of a high density of lattice defects [18]. Several methods can be used to synthesize silica shells on particle surface including the Stöber and reverse micro emulsion methods that need water as one of the media or reactants and several studies have investigated approaches to embed Quantum Dots (QDs) in silica [19]. Silica is a suitable coating material for perovskite due to its stability against environmental and chemical factors as well as good optical properties [20-21]. However, perovskite QDs can quickly decompose when contacting with polar solvents during silica synthesis process. Wang, et al. propose a solvent efficient process to synthesize green $CsPbBr_3$ perovskite quantum dots into the mesoporous silica nanocomposite by using non-polar solvent such as hexane and toluene to prevent the anion-exchange effect [22]. Dirin, et al. show insertion of perovskite precursor solutions into the pores of mesoporous leads to the template-assisted formation of perovskite nanocrystals [23]. Otherwise, offering more stable constituents of hole-transport material (HTM) for perovskite-based solar cells [24] and using the ultrafast methylamine (CH3NH2, MA)-induced defect-healing (MIDH) is necessary to improve film quality and crystalline [25].

In this paper, SiO_2 films were prepared using a simple non-vacuum process that provides fast deposition, low-cost, and large-area capability. It is shown that the improvement is due to the decrease in recombination by the high energy gap silica to block the electrons and holes. An electrospray method was utilized to prepare a $MAPbI_3$ perovskite absorption layer, and the

perovskite film was post annealed by a MA vapor to promote crystal growth and reduce defects in the film as well as remove residual solvent. The combination of SiO_2 and $MAPbI_3$ was found to be effective in improving film quality and the PCE for perovskite-based solar cells.

2. Materials and Methods

2.1. Materials

The methylamine (CH_3NH_2, 40 wt% in methanol, Panreac), hydroiodic acid (HI, 50wt% in water, Showa),and N, N-dimethylformamide (DMF, Fisher Scientific Acros) were mixed to prepare MAI precursor solution. The lead chloride ($PbCl_2$, Merc RDI 10), the lead (II) iodide (PbI_2, 98%, SHOWA), potassium hydroxide , diethyl ether (99.7 wt%, Panreac AppliChem) were used as precursor solution. The tetraethyl orthosilicate (TEOS, 98%, GC, Fluka), isopropanol alcohol (IPA, 99.99%, GC, Burdick & Jackson), ammonium water (25%, Fisher Scientific), and distilled water (Lotun Techic Rdi 10) were used to prepare SiO_2 nanoparticles. PEDOT: PSS (UniRegion-tech), high voltage power supply (30kv, 15W by YSTC), needle (26 gauge, diameter in 0.21 mm, NIPRO), syringe pump (Model-1200, KdScientific), rotary vapor (EYELA/N-1000), uvo ozone (Model NO.42A, Jelight company Inc.), and vacuum pump (Fuji Electric MBC1087G) were used to fabricate devices.

2.2. Synthesis of CH_3NH_2I and SiO_2

The CH_3NH_2I (MAI) was synthesized by adding 14 mL CH_3NH_2 40% in methanol to 15 mL hydroiodic (HI, 50 wt% in de-ionized water) and stirred for 2 h, and then put into the iced bath with further stirring for 15 min, through rotary vapor at 50 °C to precipitate the MAI then 10 mL of diethyl ether was used three times for ultrasonic cleaning . Finally, the MAI powders were obtained after the vacuum oven at 70 °C for 24h. The MAI powder XRD analysis is shown in Figure S1(a). In a typical aqueous sol-gel synthesis 1.0, 0.7, and 0.4 mL of ammonium water was dissolved with 1.5mL de-ionized water and 40 mL isopropanol alcohol in a 100 ml beaker then add 1.5 mL tetraethyl orthosilicate with stirring for 25 min. After synthesis of the precipitates was centrifuged with 14000 rpm for 5 min. The product was obtained by drying in an oven at 70 °C for 8 h, the XRD is shown in Figure S1(b) and the results of elemental atomic ratios of Si and O were very close to the expected value corresponding to the 1:2 chemical stoichiometry.

2.3. Electrospray $CH_3NH_3PbI_3$ and SiO_2

Figure S1(b) displays the electrospray system containing a high voltage power supply (20000V), a syringe and needle (26 Gauge), a syringe pump (0.5 mL/h speed), and a collector as the plate ground electrode (4cm distance). Through electrospray $CH_3NH_3PbI_3$ ($MAPbI_3$) film for 80s, then vacuum annealed at 10-2torr shows an illustration in Figure S1(d). Finally, the $MAPbI_3$ film was prepared using the methylamine (CH_3NH_2, MA) vapor-assisted diffusion shows in Figure S1(e). 3 mL of isopropanol alcohol and 2 mL de-ionized water to disperse 10 mg SiO_2 powder stirred overnight then through ultrasonic for 20 min to obtain the uniform dispersion solution.

2.4. Device fabrication

The indium tin oxide (ITO) glasses (Ruilong Photoelectric Company) were patterned as substrates. Followed by, the patterned ITO glass was sequentially cleaned using an ultrasonic treatment with detergent, de-ionized water, acetone and isopropyl alcohol thoroughly. The cleaned substrate was treated with UV/ozone for 30 min, coated with PEDOT:PSS at 4000 rpm for 60 s, and dried on a hot plate at 150 °C for 15 min. A mesoporous SiO_2 layer is prepared by electrospray SiO_2 dispersion solution with the power voltage was 6600V, a syringe speed was 0.3 mL/h, and the working distance was 4 cm at 90 °C. Afterwards, PbI_2 solution was sprayed onto SiO_2 layer to form PbI_2 film, and MAI vapor was further reacted with the PbI_2 film to form the $MAPbI_3$ perovskite film. The perovskite film was recrystallized in the vacuum using the CH_3NH_3I/KOH (1:1) mixture to produce methylamine vapor

enhanced without DI water. The $CH_3NH_3PbI_3$ solar cell device was completed by physical vapor deposition (PVD) of the electron transport layer (C60, 30 nm), the hole blocking layer (BCP, 10 nm), and the electrode (Al, 100 nm). The structure of device is composed of Glass/ITO/PEDOT: PSS/SiO_2/$MAPbI_3$/C60/BCP/Al.

2.5. Characterizations

The crystalline structures of products were analyzed using X-ray Diffraction (Bruker D8 Advance). The morphology of SiO_2 and $MAPbI_3$ were characterized by Scanning Electron Microscope (Hitachi S-3000N). Besides, Atomic Force Microscopic (AFM) was utilized to measure surface roughness of the films on a MultiMode AFM with Nanoscope-V controller (Bruker, Santa Barbara, CA, USA). UV–Vis spectra were taken by a spectrometer (PerkinElmer Lambda 7500, Waltham, MA, USA) to investigate the optical properties. Particle size was analyzed by Nanotrac NPA-150. The current density-voltage (J-V) curves were carried out in a nitrogen-filled glove box using a Keithley 2400 Source Meter under the standard 1 sun AM 1.5G simulated irradiation (100mWcm−2) from a Newport 91160 A 300W Solar Simulator (Class A). To adjust the light intensity of the illumination, the neutral density filter was placed in front of the device during the measurement. Schott visible-color glass-filtered (KG5 color filter) Si diode (Hamamatsu S1133) was utilized to correct the simulated solar irradiance.

3. Results and discussion

All the electrospray $MAPbI_3$ experimental parameters are given in Table 1. Different concentrations of precursors were separately investigated (7, 8, 9 and 10 weight percentage of 1 mL DMF). The EDS analysis indicate that $MAPbI_3$ film obtained at 7 wt % was chloride free after vacuum annealing for 30 min for $MAPbI_3$ film deposited at 8 wt% and 9wt% the sample becomes chloride free after vacuum annealing for 40 min, and 50 min, respectively.

3.1. Morphology of $MAPbI_3$ film

The surface morphologies of $MAPbI_3$ film was examined by SEM, and the results are shown in Figure 1. Figure 1(a)~(d) show a rod-shaped crystal with poor film coverage obtained at film annealing at 90 ℃ when the concentration ratios of 7, 8, 9, and 10wt%. When the electrospray temperature increased to 110 ℃ the $MAPbI_3$ films become relatively stable and formed a better quality film (Figure 1(e)~(h)). $MAPbI_3$ film deposited at 110 ℃ consist of nanofibers with a minor amount of spherical shape and gradually changing to flakes with an increasing temperature of 130 ℃, with complete coverage film as shown in Figure 1(i)~(l). However, the surface morphology exhibited faceted surface voids before MA treatment. SEM images of $MAPbI_3$ deposited at different concentration after MA treatment at 110 ℃ (Figure S2). The surface roughness of the films was determined by AFM for a scanning area 30 × 30 μm as shown in Figure S3. Our experimental results indicated the roughness ranges were 113, 138, 147, 116 for $MAPbI_3$ deposited using various precursor concentration 7, 8, 9, and 10 wt%, and from 138 to 57 nm with MA vapor-assisted, respectively. As shown in Figure S3, $MAPbI_3$ film is well grown in the grains boundaries, and the roughness decreased progressively from the island-needle structure transition to smooth film.

3.2. Morphology of SiO_2 nanoparticles

The morphology of SiO_2 nanoparticles was characterized by SEM, as shown in Figure 2. Figure 2(a)~(e) shows the regular SiO_2 particles formed when the amount of ammonium water increases along with reaction time. The shapes of Figure 2(f)~(h) are minor particles and flakes. With increasing the ammonium concentration and improved the crystallinity resulting in a more regular morphology. The formation mechanism of the precipitates causes the flakes to become sheets and sheets to spheres. The average size of particle size distribution of 0.7 mL ammonium water reacted for 75 min was 92.6nm shows in Figure 2(j), and the detailed data shows in table S1. Hwang, et al. [26] reported it is necessary to limit the particles size was below 70 nm in order to stabilize the power conversion efficiency while maintaining favorable optical properties. Hence, we prepared using the recipe with 0.7 mL ammonium water reacted for 25 min for spraying $MAPbI_3$ film.Table 1. Experimental parameters and the element ratios of the resulting MAPbI3 film through the hotplate for 60 min and vacuum annealing at 110 ℃.

Wt % \ Elemental atomic%				Hotplate 60 min	Vacuum 20 min	Vacuum 30 min	Vacuum 40 min	Vacuum 50 min
7 wt%	MAI (mg)	25.7	Cl	11.89	1.64	0	0	0
	PbI_2 (mg)	45.3	I	88.11	98.36	100	100	100
8 wt%	MAI (mg)	30	Cl	18.81	9.26	5.74	0	0
	PbI_2 (mg)	52	I	81.19	90.74	94.26	100	100
9 wt%	MAI (mg)	32.7	Cl	14.76	5.66	2.84	1.43	0
	PbI_2 (mg)	59.3	I	85.24	94.34	97.16	98.57	100
10 wt%	MAI (mg)	38	Cl	15.23	10.99	1.51	1.32	0
	PbI_2 (mg)	67	I	84.77	89.01	98.49	98.68	100

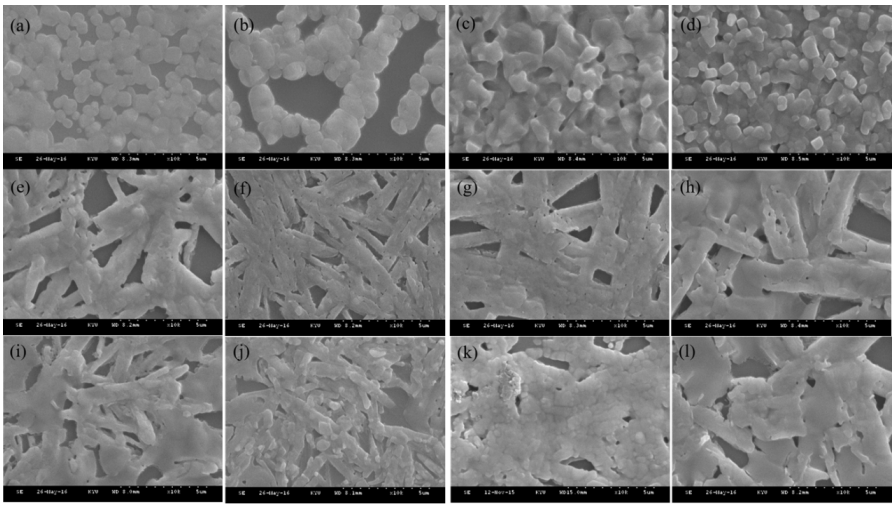

Figure 1. SEM images of electrospray $MAPbI_3$ film under vacuum annealing temperature at 90 °C of various precursor ratios (a) 7wt%, (b) 8wt%, (c) 9wt%, (d) 10wt%, at 110 °C (e) 7wt% (f) 8wt%, (g) 9wt%, (h) 10wt%, at 130 °C (i) 7wt%, (j) 8wt%, (k) 9wt%, (l) 10wt%.

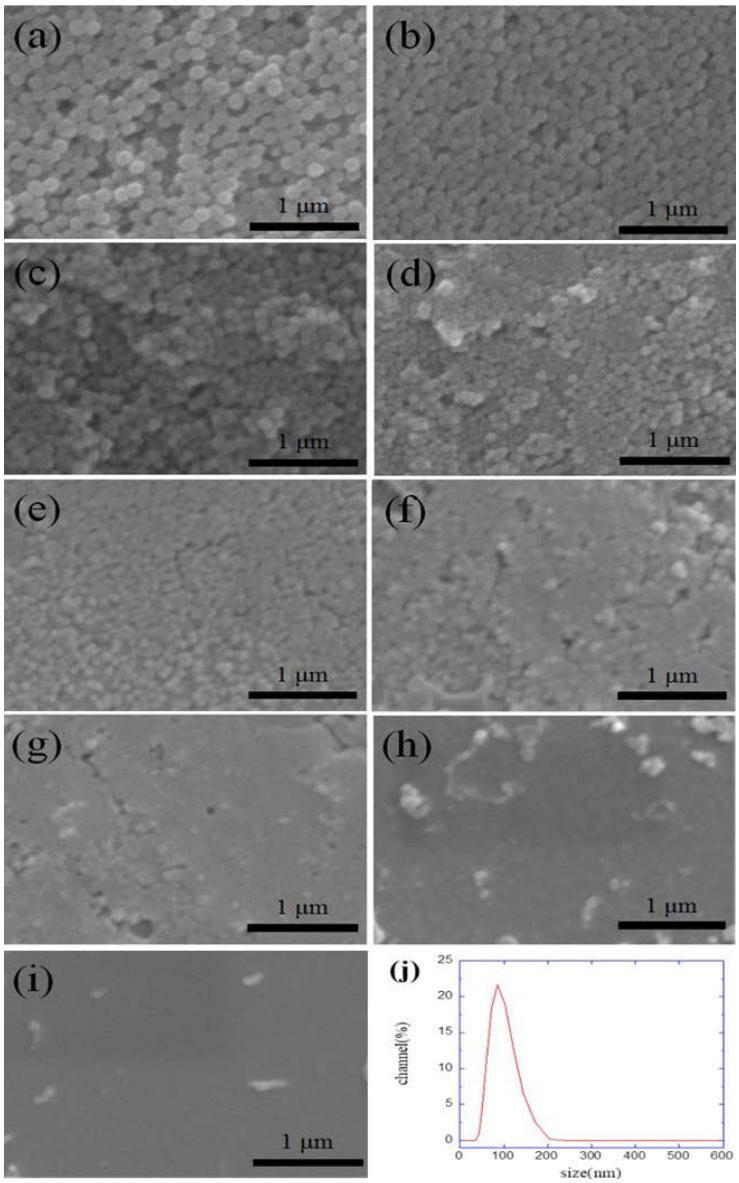

Figure 2. SEM morphology of SiO_2 powders obtained with various ammonium water concentration of 1.0 mL reacted for (a) 75 min, (b) 50 min, (c) 25 min, 0.7 mL reacted for (d) 75 min, (e) 50 min, (f) 25 min, 0.4 mL reacted for (g) 75 min, (h) 50 min, (i) 25 min, and (j) particle size distribution of 0.7 mL ammonium water reacted for 75 min.

3.3. Morphology of SiO_2 with $MAPbI_3$ multilayer

It has been reported that the DMF reacts with PEDOT:PSS and decrease power conversion efficiency [27]. Therefore, we insert SiO_2 blocking layer on PEDOT:PSS (Figure 3). Therefore, the coordination is a critical factor for the synthesis of $MAPbI_3$. When spray $MAPbI_3$ without SiO_2, there is needle-like structure with increase in the spraying time leading to full film coverage. However, excessive amounts of SiO_2 cause the increase of intrinsic resistance within the solar cells. On the other hand, under this condition there are many voids with naked eye, where $MAPbI_3$ were sprayed onto the smaller SiO_2 particles to serve as a recombination site in the system as shown in Figure S4.

3.4. The electrospray device and vapor-assisted

The XRD pattern of the tetragonal $MAPbI_3$ with 8 wt% concentration by annealing treatment at 90, 110, 130 °C are shown in Figure S5. The $MAPbI_3$ annealed at temperature at 90 °C resulted in formation of secondary phases PbI_2 with the intensity of MAPbI3 peak increases along with the temperature. To explore the effect of MA sublimation heat diffusion on the formation of the $MAPbI_3$, XRD measurements were performed and plotted in Figure 4. The XRD patterns show perovskite-phase peaks at

14.14°, 28.45°, 32.99°, 43.24°, and 47.35°, assigning to the (110), (220), (310), (224), and (314) planes of the tetragonal $MAPbI_3$ crystal structure [3]. The MA vapor-assisted recrystallization increased the peak intensity and promoted the crystal growth.

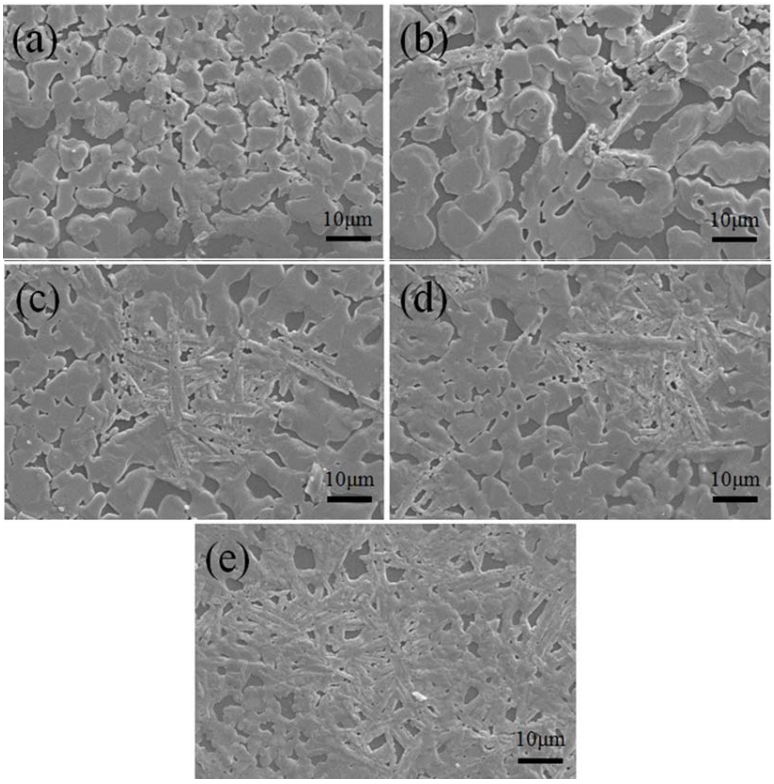

Figure 3. Surface morphologies of spraying 8wt% $MAPbI_3$ film with annealing at 110 ℃ onto the SiO_2 dispersion (a) without SiO_2, (b) 5s, (c) 15s, (d) 25s, and (e) 35s.

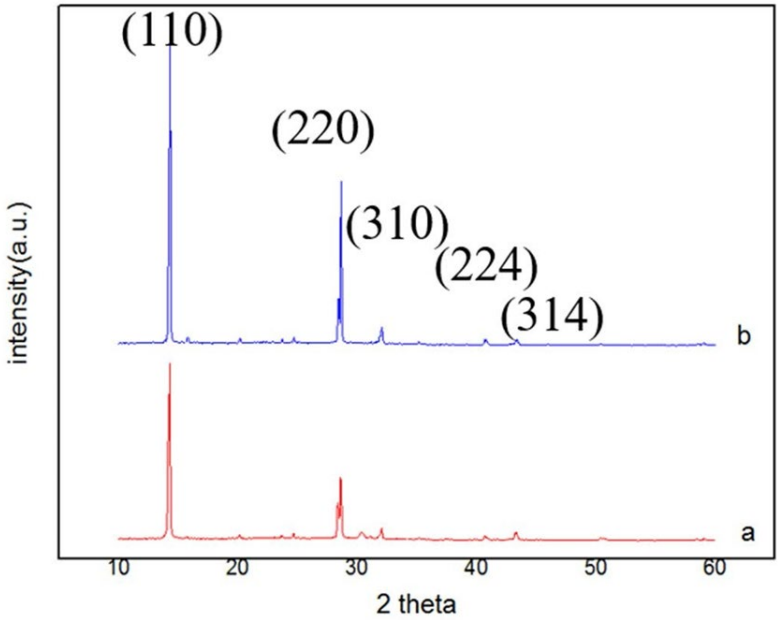

Figure 4. XRD pattern of vacuum annealing of 8wt % in different temperature at 110 ºC (a) without MA vapor-assisted, (b) with MA vapor-assisted.

3.5. Optical Absorption

The UV-visible absorption spectrum results for the SiO_2 spraying various time onto the tetragonal 8 wt% $MAPbI_3$ film are shown in Figure 5. The perovskite without the SiO_2 spraying has a high absorption at the wavelength greater than 760 nm. It can be seen that spray SiO_2 film decrease $MAPbI_3$ film absorbed in NIR wavelength and enhanced the UV-vis light absorption, and this fact can be ascribed to the improved adhesion between PEDOT:PSS and $MAPbI_3$ film as shown in Figure 5(a). It is apparent that a high surface area from the SiO_2 coating enhances the UV-visible light absorption. Among the samples, the spraying time for 15 s exhibited the most significant UV-visible light absorption enhancement.

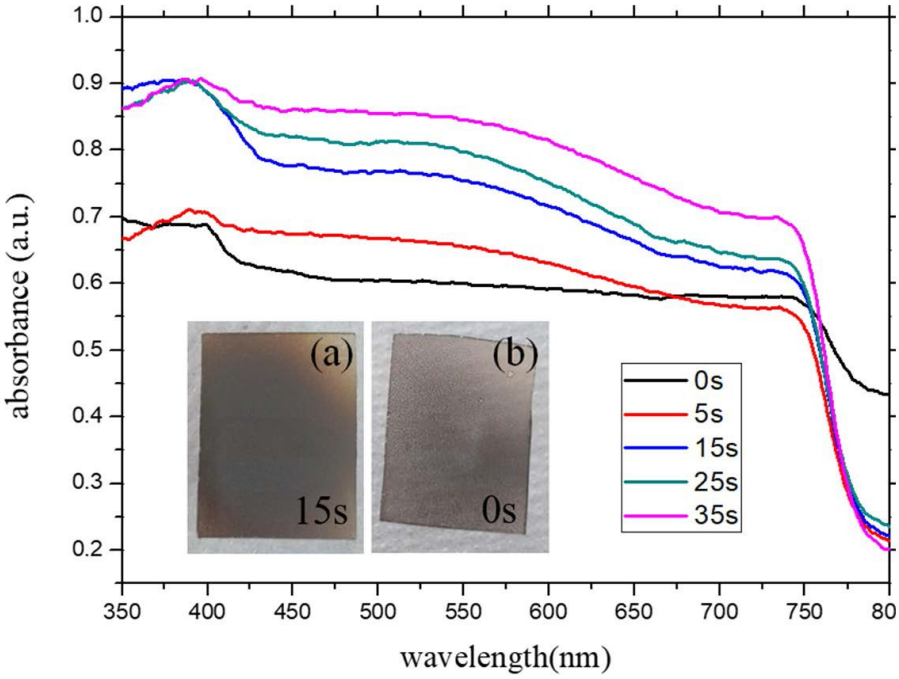

Figure 5. UV–Vis absorption spectroscopy by the SiO_2 spraying various time onto the 8 wt% $MAPbI_3$ film and inset: the surface adhesion of the spraying SiO_2 (a) 15s, (b) 0s.

3.6. PCE

The current density–voltage (J–V) curves performed under the standard 1 sun AM 1.5G simulated solar irradiation was shown in Figure 6. The photovoltaic parameters exhibited a Voc of 0.55 V, a Jsc of 14.56 mA/cm^2, and a FF of 0.39, corresponding to a PCE of 3.15% without SiO_2 coating for the glass/ITO/PEDOT:PSS/8 wt% $MAPbI_3$/C60/BCP/Al device, and a Voc of 0.86, 0.89,0.72, and 0.64 V, a JSC of 15.18, 19.89, 19.36, and 14.34 mA/cm^2, and a FF of 0.42, 0.50, 0.48, and 0.48 corresponding to a PCE of 5.48, 8.85, 6.69, and 4.41% for the glass/ITO/PEDOT:PSS/SiO_2/8 wt% $MAPbI_3$/C60/BCP/Al device of electrospun SiO_2 for 5, 15, 25, and 35 s, respectively. All the cell performances were listed in Table 2. We obtained the 15s spinning SiO_2 has the highest PCE according to the uniform morphology and best absorption below 400 nm. Besides, the power conversion efficiency of 8 wt% perovskite device was compared in different temperature with 90 °C(Fi,g1u1re0 S°C6, aanndd 130 °C table S2) and different concentration of 7 wt%, 8 wt%, 9 wt%, 10wt% under vacuum annealing at 110 °C (Figure S7 and table S3). Figure 7 clarified the energy levels for each layer, composed of glass/ITO/ PEDOT:PSS/SiO_2/ $MAPbI_3$/C60/BCP/Al. The SiO_2 was deposited on PEDOT:PSS exhibits a work function energy level of 4.8–5.2 eV [29-30], after the electrons generated in the $MAPbI_3$ conduction band which avoid jumped to the SiO_2. Moreover, the energy barriers at VB and conduction band CB edge levels of $MAPbI_3$ with BCP and SiO_2 film deposited onto PEDOT:PSS, respectively, would block the transport of the holes and electrons to reach the electrodes.

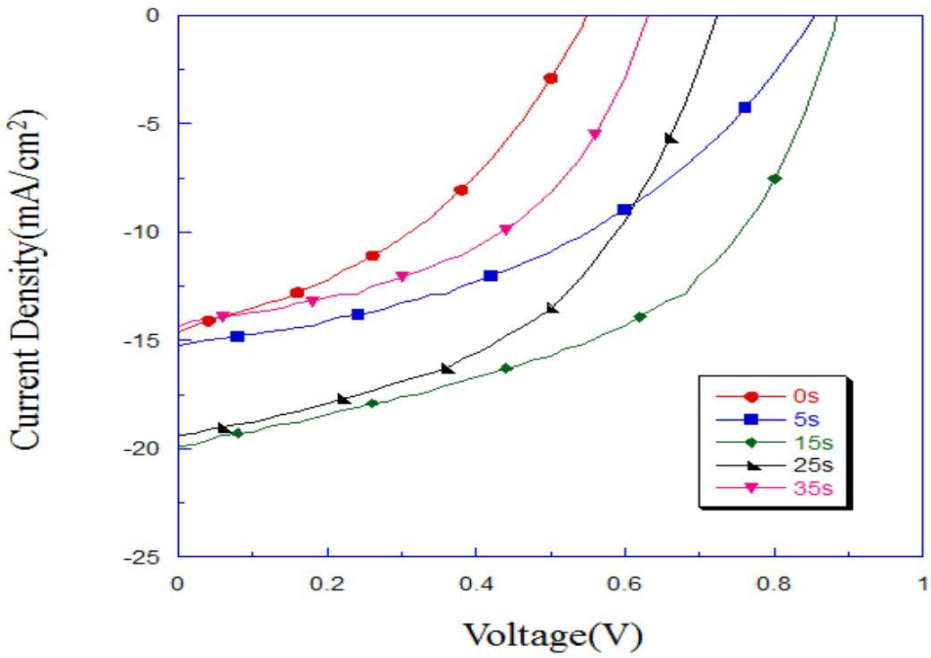

Figure 6. I-V curve of 8 wt% perovskite device in various time of spray SiO_2 without SiO_2, 5, 15, 25, and 35s.

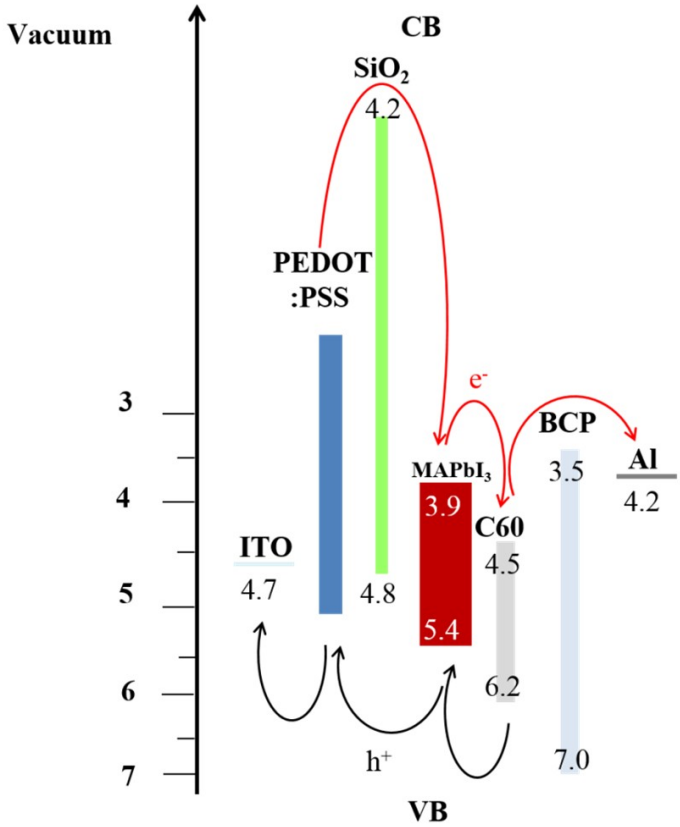

Figure 7. Schematic diagram for proposed of a glass/ITO/PEDOT:PSS/ SiO_2/$MAPbI_3$ with MA vapor-assisted/C60/BCP/Al structure.

Table 2. Photovoltaic parameters calculated from the J-V curves in Figure 6.

DevicesSpray SiO_2	Jsc (mA/cm^2)	Voc (V)	FF	η(%)
Without SiO_2	14.56	0.55	0.39	3.15
5S	15.18	0.86	0.42	5.48
15S	19.89	0.89	0.50	8.85
25S	19.36	0.72	0.48	6.69
35S	14.34	0.64	0.48	4.41

4. Conclusion

We concluded that SiO_2 scaffold layer between PEDOT:PSS and $MAPbI_3$ would block the transport of the holes and electrons to reach the electrodes. The crystallinity of $MAPbI_3$ film was increased through MA vapor-assisted method. Furthermore, it was found that adding SiO_2 scaffold layer not only enhanced the broad light absorption region from ultraviolet to near-infrared, but also prevented the recombination of electron-hole pairs and improved the charge transfer processes. The result shows the best performing device was fabricated using of 4.54 mmol ammonium water to form SiO_2 spray 15 s with an open-circuit voltage of 0.89V, a current density of 19.89 mA/cm^2, a fill factor of 0.50, and a power-conversion efficiency of 8.85%.

Author Contributions: C.C.H. wrote and revised the manuscript. T.Y.T. and C.W.C. conducted the fabrication and characterization of devices. Y.S.F revised the manuscript. All of the authors reviewed and contributed to the manuscript.

Funding: This research was funded by Ministry of Science and Technology of Taiwan (MOST) and the Southern Taiwan Science Park Bureau, MOST, Taiwan, R.O.C., Grant No. NSC 109-2113-M-024 -001 -, NSC 108-2113-M-024 -001- and 106GF01.

Acknowledgments: The authors thank Department of Photonics, National Cheng Kung University (NCKU)

Conflicts of Interest: The authors declare no conflict of interest.

References

1. C. Wehrenfennig, G. E. Eperon, M. B. Johnston, H. J. Snaith, L. M. Herz, High charge carrier mobilities and lifetimes in organolead trihalide Perovskites, *Adv. Mater*. **2014,** *26,* 1584-1589.
2. A. Kojima, K. Teshima, Y. Shirai, T. Miyasaka, Organometal halide perovskites as visible light sensitizers for photovoltaic cells, *J. Am. Chem. Soc.* **2009**, *131,* 6050–6051.
3. D. Bi, C. Yi, J. Luo, J. -D. Décoppet, F. Zhang, S. M. Zakeeruddin, X. Li, A. Hagfeldt, M. Grätzel, Polymer-templated nucleation and crystal growth of perovskite films for solar cells with efficiency greater than 21%, *Nature Energy* **2016,** *1,* 16142.
4. W.S. Yang, B.-W. Park, E.H. Jung, N.J. Jeon, Y.C. Kim, D.U. Lee, S.S. Shin, J. Seo, E.K. Kim, J.H. Noh, S. Il Seok, Iodide management in formamidinium-lead-halide based perovskite layers for efficient solar cells, *Science* **2017**, *356,* 1376–1379.
5. J.Y. Jeng, Y.F. Chiang, M.H. Lee, S.R. Peng, T.F. Guo, P. Chen, T.C. Wen, $CH_3NH_3PbI_3$ perovskite/fullerene planar-heterojunction hybrid solar cells, *Adv. Mater*., **2013**, *25*, 3727-3732.
6. F. Xu, T. Zhang, G. Li, Y. Zhao, Synergetic Effect of Chloride Doping and $CH_3NH_3PbCl_3$ on $CH_3NH_3PbI_3$-xClx Perovskite-Based Solar Cells, *ChemSusChem Comm*., **2017**, *10*, 2365-2369.
7. G. C. Xing, N. Mathews, S. Y. Sun, S. S. Lim, Y. M. Lam, M. Gr¨atzel, S. Mhaisalkar, T. C. Sum, Long-Range balanced electronand hole-transport lengths in organic-inorganic $CH_3NH_3PbI_3$, *Science* **2013**, *342*, 344-347.
8. J. H. Im, C. R. Lee. J. W. Lee, S. W. Park, N. G. Park. 6.5% efficient perovskite quantum-dot-sensitized solar cell. *Nanoscale*, **2011**, *3*, 4088-4093.
9. Q. Chen, H. Zhou, Z. Hong, S. Luo, H. S. Duan, H. H. Y. Liu, G. Li, Y. Yang, Planar heterojunction Perovskite solar cells via vapor-assisted solution process. *Journal of the American Chemical Society*, **2014**, *136*, 622-625.
10. Z. Xiao, C. Bi, Y. Shao, Q. Dong, Q. Wang, Y. Yuan, C. Wang, Y. Gao, J. Huang. Efficient, High yield Perovskite Photovoltaic Device Grown by Interdiffusion of solution-Processed Precursor Stacking Layers. *Energy & Environment Science*, **2014**, *7*, 2619-2623.
11. Z. Zhou, Z. Wang, Y. Zhou, S. Pang, D. Wang, H. Xu, Z. Liu, N. P. Padture, G. Gui. Methylamine-Gas-Induced Defect-Healing Behavior of $CH_3NH_3PbI_3$ Thin Films for Perovskite Solar Cells. *Angewandte International Chemie*, **2015**, *54*, 9705-9709.

12. H. Chen, F. Ye, J. He, M. Yin, Y. Wang, F. Xie, E. Bi, X. Yang, M. Grätzel, L. Han. A solvent- and vacuum-free route to large-area perovskite films for efficient solar modules. *Nature*, **2017**, *550*, 92-95.
13. S. Y. Lin, T. S. Su, T. Y. Hiseh, P. C. Lo, T. C. Wei. Efficient Plastic Perovskite Solar Cell with a Low-Temperature Processable Electrodeposited TiO_2 Compact Layer and a Brookite TiO_2 Scaffold. *Advanced Energy Materials*, **2017**, *7*, 1700169.
14. G. E. Eperon, S. D. Stranks, C. Menelaou, M. B. Johnston, L. M. Herz, H. J. Snaith. Formamidinium lead trihalide: a broadly tunable perovskite for efficient planar heterojunction solar cells. *Energy & Environmental Science*. **2014**, *7*, 982-988.
15. S. S. Mali, C. K. Hong, A. I. Inamdar, H. Imb, S. E. Shim. Efficient planar n-i-p type heterojunction flexible perovskite solar cells with sputtered TiO_2 electron transporting layers. *Nanoscale*, **2017**, *9*, 3095-3104.
16. M. M. Lee, J. Teuscher, T. Miyasaka, T. N. Murakami, H. J. Snaith. Efficient hybrid solar cells based on meso-superstructured organometal halide Perovskites, *Science*, **2012**, *338*, 643–648.
17. J. Duan, J. Wu, J. Zhang, Y. Xu, H. Wang, D. Gao, P. D. Lund. TiO_2/ZnO/TiO_2 sandwich multi-layer films as a holeblocking layer for efficient perovskite solar cells. *International Journal of Energy research*, **2016**, *40*, 806-813.
18. N. Yi, Y. Cao, Y. Su, W. L. Dai, H. Y. He, K. N. Fan. Nanocrystalline $LaCoO_3$ perovskite particles confined in SBA-15 silica as a new efficient catalyst for hydrocarbon oxidation. *Journal of catalysis*, **2005**, *230*, 249-253.
19. C. Sun, Y. Zhang, C. Ruan, C. Yin, X. Wang, Y. Wang, W. W. Yu. Efficient and Stable White LEDs with Silica-Coated Inorganic Perovskite Quantum Dots. *Advanced Materials*, **2016**, *28*, 10088-10094.
20. I. Rivas, J. Alvarez, E. Pietri, M. J. P'erez-Zurita, M. R. Goldwasser. Perovskite-type oxides in methane dry reforming: Effect of their incorporation into a mesoporous SBA-15 silica-host. *Catalysis Today*, **2010**, *149*, 388-393.
21. A. Lita, A. L. Washington II, L. V. D, Burgt, G. F. Strouse, A. E. Stiegman. Stable Efficient Solid-State White-Light-Emitting Phosphor with a High Scotopic/Photopic Ratio Fabricated from Fused CdSe–Silica Nanocomposites. *Advanced Materials*, **2010**, *22*, 3987-3991.
22. H. C. Wang, S. L. Lin, A. C. Tang, B. P. Singh, H. C. Tong, C. Y. Chen, Y. C. Lee, T. L. Tsai, R. S. Liu. Mesoporous Silica Particles Integrated with All-Inorganic $CsPbBr_3$ Perovskite Quantum-Dot Nanocomposites (MP-PQDs) with High Stability and Wide Color Gamut Used for Backlight Display. *Angewandte Chemie International Edition*, **2016**, *55*, 7924-7929.
23. D. N. Dirin, L. Protesescu, D. Trummer, I. V. Kochetygov, S. Yakunin, F. Krumeich, N. P. Stadie, M. V. Kovalenko. Harnessing Defect-Tolerance at the Nanoscale: Highly Luminescent Lead Halide Perovskite Nanocrystals in Mesoporous Silica Matrixes. *Nano Lett*. **2016**, *16*, 5866-5874.
24. M. Yuan, X. Zhang, J. Kong, W. Zhou, Z. Zhou, Q. Tian, Y. Meng, S. Wu, D. Kou. Controlling the Band Gap to Improve Open-Circuit Voltage in Metal Chalcogenide based Perovskite Solar Cells. *Electrochim. Acta*, **2016**, *215*, 374-379.
25. Z. Zhou, Z. Wang, Y. Zhou, S. Pang, D. Wang, H. Xu, Z. Liu, N. P. Padture, G. Cui. Methylamine-Gas-Induced Defect-Healing Behavior of $CH_3NH_3PbI_3$ Thin Films for Perovskite Solar Cells. *Angewandte Chemie International Edition*, **2015**, *54*, 9705-9709.
26. S. H. Hwang, J. Roh, J. Lee, J. Ryu, J. Yun, J. Jang. Size-controlled SiO2 nanoparticles as scaffold layers in thin-film perovskite solar cells. Journal of Materials Chemistry A, **2014**, *2*, 16429-16433.
27. J. H. Huang, D. Kekuda, C. W. Chu, K. C. Ho. Electrochemical characterization of the solvent-enhanced conductivity of poly(3,4 ethylenedioxythiophene) and its application in polymer solar cells. *Journal of Materials Chemistry*, **2009**, *19*, 3704– 3712.
28. A. Radivo, E. Sovernigo, M. Caputo, S. D. Zilio, T. Endale, A. Pozzato, A. Goldonid, M. Tormen. Patterning PEDOT:PSS and tailoring its electronic properties by water-vapour-assisted nanoimprint lithography. *Royal Society of Chemistry Advances*, **2014**, *4*, 34014-34025.
29. P. A. Lane, P. J. Brewer, J. Huang, D. D. C. Bradley, J. C. deMello. Elimination of hole injection barriers by conducting polymer anodes in polyfluorene light-emitting diodes. *Physical Review B*, **2006**, *74*, 125320.
30. C. Tengstedt, W. Osikowicz, W. R. Salaneck, I. D. Parker, C. H. Hsu. Fermi-level pinning at conjugated polymer interfaces. *Applied Physics Letters*, **2006**, *88*, 053502.

Figures

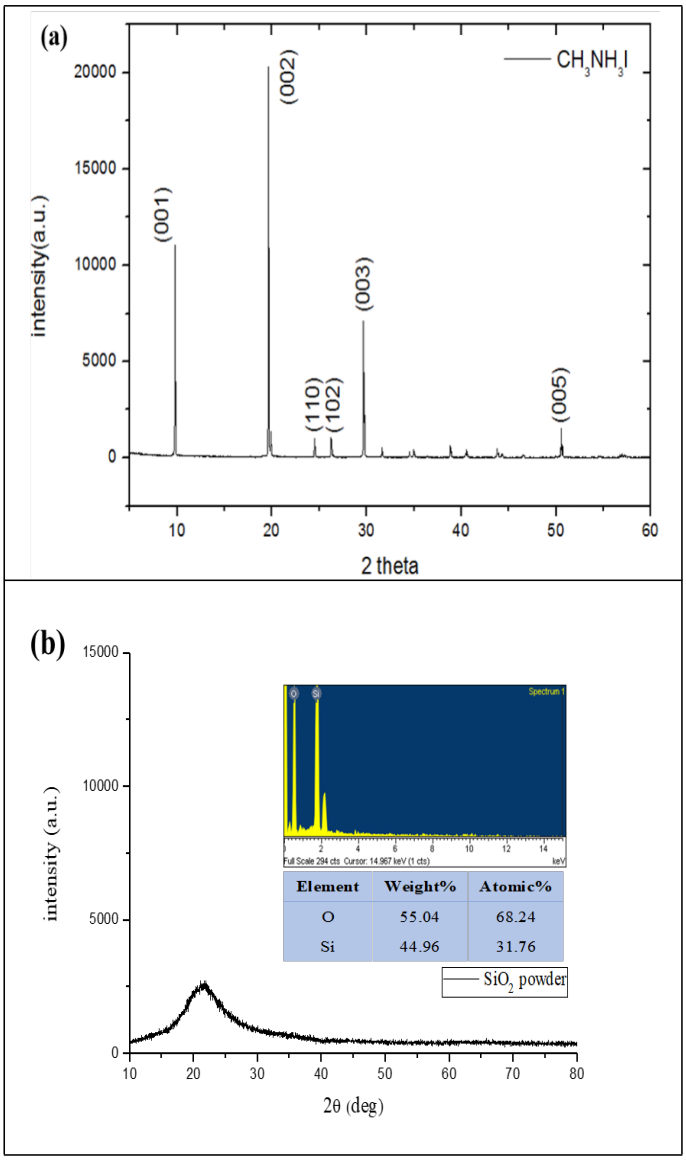
(a)
CH3NH3I
(001)
(002)
(110)
(102)
(003)
(005)
intensity(a.u.)
2 theta
(b)
intensity (a.u.)
2θ (deg)
SiO2 powder
Element | Weight% | Atomic%
O | 55.04 | 68.24
Si | 44.96 | 31.76

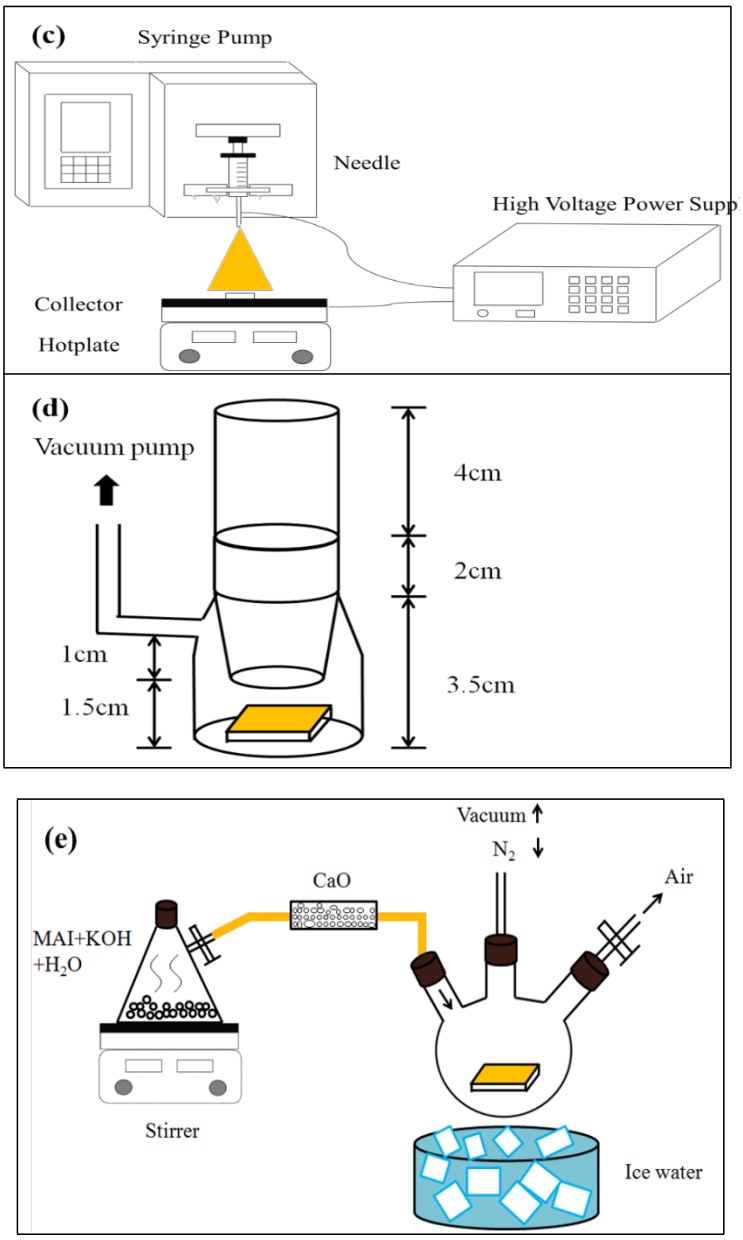

Figure S1. Schematic illustration of (a) XRD spectrum of synthesize CH_3NH_2I powder (b) XRD spectrum of synthesize silica powder and the EDS analysis (c) electrospray $CH_3NH_3PbI_3$ film (d) after electrospray $CH_3NH_3PbI_3$ film to anneal in a vacuum system (e) then via CH_3NH_2 vapor-assisted treatment in a 100 mL three-neck flask vacuum system.

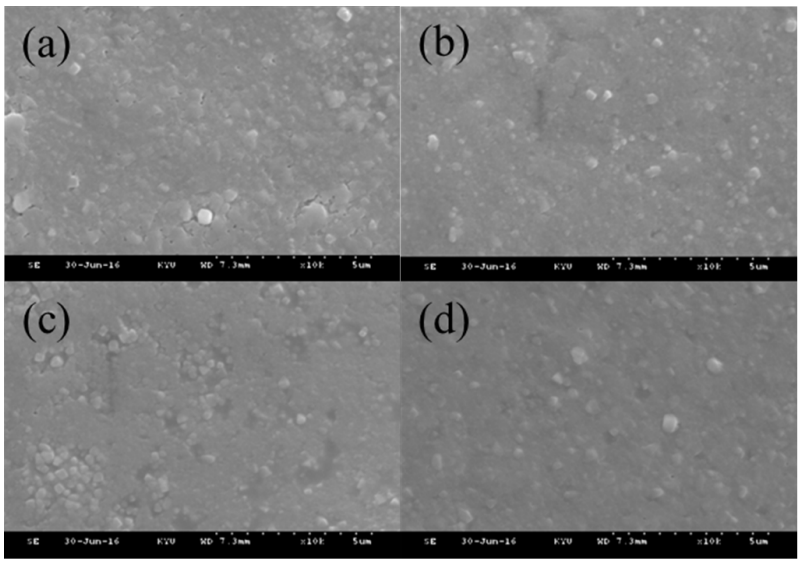

Figure S2. SEM images of MAPbI3 after MA-treated in different concentration at 110℃ (a) 7wt%, (b) 8wt%, (c) 9wt%, (d) 10wt%.

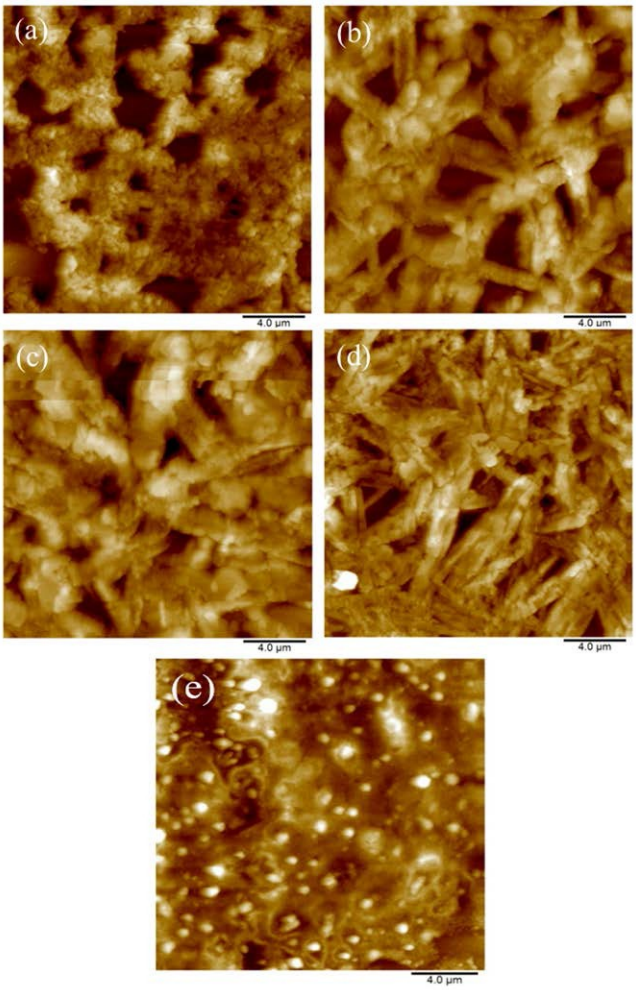

Figure S3. AFM images of MAPbI3 in different concentration at 110℃ (a) 7wt%, (b) 8wt%, (c) 9wt%, (d) 10wt%, (e) 8wt % after MA-treated.

Table S1. Particle size distribution calculated based on the sample was charged of 0.7 mL ammonium water reacted for 75min.

Size (nm)	Channel (%)	Total (%)
204.4	0.35	100
171.9	2.69	99.65
144.5	6.63	96.96
121.5	12.93	90.33
102.2	19.18	77.4
85.9	21.88	58.22
72.3	18.7	36.34
60.8	11.5	17.64
51.1	4.93	6.14
43.0	1.21	1.21
Average size: 92.6nm		

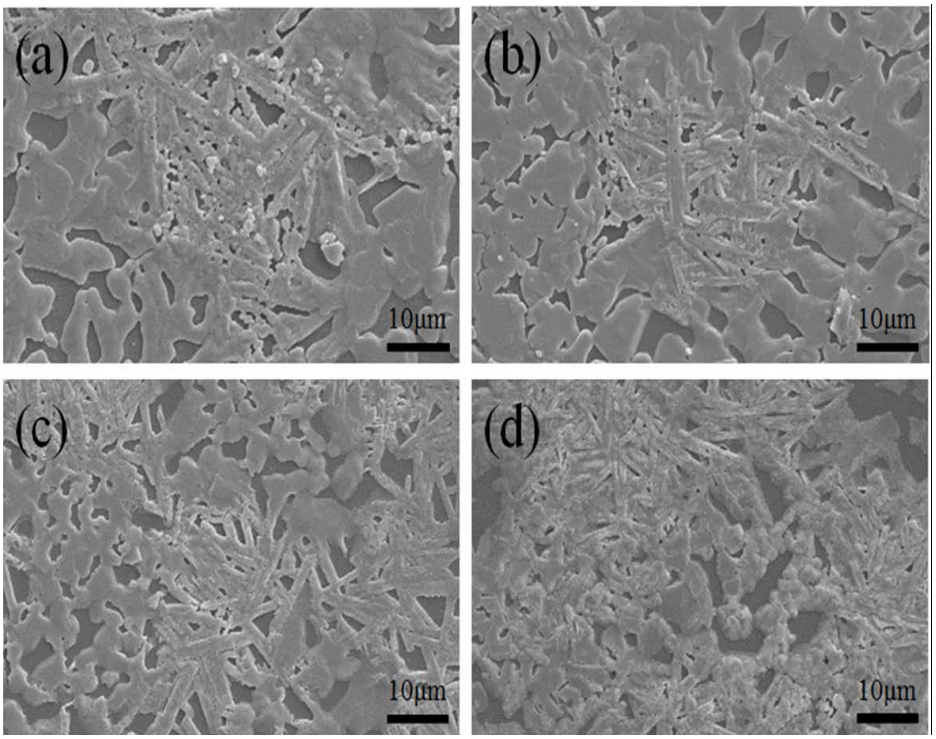

Figure S4. Surface morphologies of spraying 8wt% MAPbI3 film with annealing at 110℃ onto the 0.7 mL ammonium water reacted (a) 50 min, (b) 25min, 0.7 mL ammonium water reacted (c) 75min, (d) 50min for spraying SiO2 dispersion 15s.

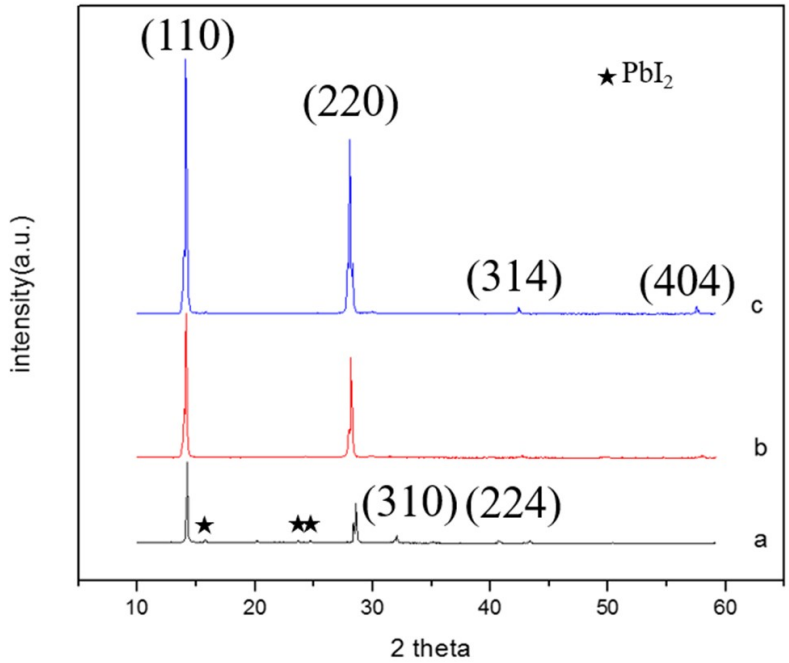

Figure S5. XRD pattern of 8 wt% $CH_3NH_3PbI_3$ vacuum annealing under different temperature (a) 90 °C, (b) 110 °C, and (c) 130 °C.

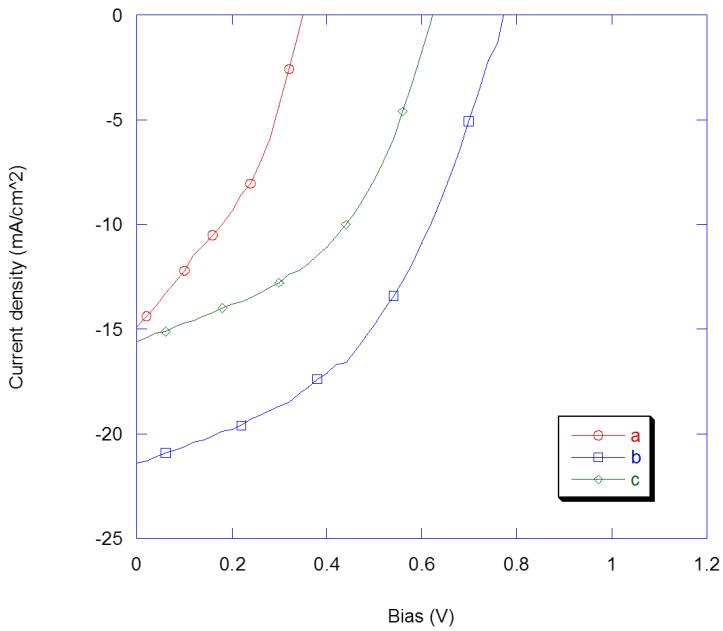

Figure S6. 8 wt% I-V curve of perovskite device in different temperature (a) 90 °C, (b) 110 °C, (c) 130 °C.

Table S2. Photovoltaic parameters calculated from the J-V curves in Fig. S6.

Temperature	90 ℃	110 ℃	130 ℃
Voc (V)	0.35	0.78	0.62
Jsc (mA/cm^2)	14.91	21.41	15.57
FF	0.37	0.44	0.46
PCE (%)	1.93	7.40	4.46

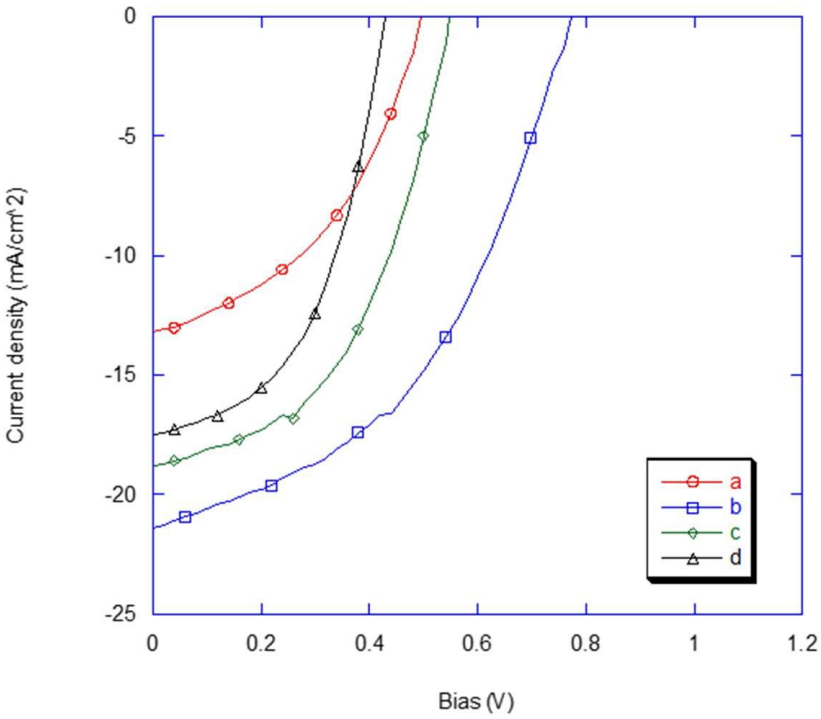

Figure S7. I-V curve of perovskite device in different concentration under vacuum annealing at 110℃ (a) 7wt%, (b) 8wt%, (c) 9wt%, (d) 10wt%.

Table S3. Photovoltaic parameters calculated from the J-V curves in Fig. S7.

Concentration	7wt %	8wt%	9wt%	10wt%
Voc (V)	0.51	0.78	0.55	0.43
Jsc (mA/cm^2)	16.41	21.41	18.80	17.48
FF	0.47	0.44	0.49	0.50
PCE (%)	3.92	7.4	5.01	3.73